Journal of Environmental Statistics
April 2020, Volume 9, Issue 6. http://www.jenvstat.org

A Mouse Model For Studying Fire Spread Rates Using Experimental Micro-fires

John R.J. Thompson
Wilfrid Laurier University

Xi J. Wang
UBC Okanagan

W. John Braun
UBC Okanagan

Abstract

We outline the design of a fire spread smoldering apparatus and methodology for experimental micro-fires that allow for the exploration of the effects of environmental covariates on fire spread rate and fire spotting rate distributions. The fire smoldering experiments are measured using a digital camera at a birds-eye view above the experiment. The movies are segmented and processed using anisotropic diffusion and data-sharpening to capture the ignition and extinction times of individual pixels. We demonstrate how the processed data can be used to estimate fire rate of spreads for fire spread models using nonparametric kernel regression.

Keywords: anisotropic diffusion, data sharpening, experiments, firebrand spotting rates, forest fires, fire image processing, fire spread rates, kernel smoothing, nonparametric statistics.

1. Introduction and background

Fire spread is a complex natural physical process and stochastic fire spread models require estimated fire spread rates based on environmental conditions such as weather, topography, fuel type, and moisture level. Fire spread rates are notoriously difficult to predict due to the variability of actual fire spread rates as a result of the complex, large-scale physical spread phenomena of fire spread (Cruz and Alexander 2013). In the medical sciences, mice have a similar genetic make-up to humans and are used in a laboratory environment as an experimental model for diseases to understand how these diseases affect and may be treated in human patients. The common term for this type of medical research is “mouse model”

(Couffinhal, Silver, Zheng, Kearney, Witzenbichler, and Isner 1998). In this paper, we outline a micro-fire smoldering apparatus that is a "mouse" model to forest fires, and a statistical methodology to estimate fire growth rates and rate variability. We apply computer vision techniques to analyze the fire spread measurements from the apparatus. The objective of this research is to develop the statistical tools to study the mouse model fire growth patterns, with future plans to apply those tools to forest fires.

The study of forest fire spreads using data obtained through laboratory experiments is an ongoing study of the complex physical process of forest fires. Previous experimental fire apparatus studies have used a variety of fuel beds to study fire spread under a variety of environmental conditions in the experimental setting. Some example experimental apparatus research in forest fires are vertical white birch sticks arranged in a rectangular grids (Hwang and Xie 1984; Wolff, Carrier, and Fendell 1991; Weise and Biging 1994), compressed paper sticks with cotton on the floor and canopy (Buscarino, Famoso, Fortuna, Frasca, and Xibilia 2015), laser-cut cardboard to study the structure of fire and fire spread (Finney, Forthofer, Grenfell, Adam, Akafuah, and Saito 2013; Finney, Forthofer, and Grumstrup 2017), match-stick arrays to study linear fire spread (Fons 1946; Vogel and Williams 1970; Prahl and Tien 1973), match splits (Wolff *et al.* 1991; Beer 1993, 1995), excelsior (Catchpole, Catchpole, Butler, Rothermel, Morris, and Latham 1998), pine needles (Rothermel and Anderson 1966), ponderosa pine lathes (Finney, Cohen, Forthofer, McAllister, Gollner, Gorham, Saito, Akafuah, Adam, and English 2015), and optical lens tissue paper soaked with potassium nitrate (Zhang, Zhang, Alstøm, and Levinsen 1992; Maunuksela, Myllys, Kähkönen, Timonen, Provatas, Alava, and Ala-Nissila 1997; Maunuksela, Myllys, Timonen, Alava, and Ala-Nissila 1999). An excellent review of empirical and quasi-empirical fire spread apparatus was written by Sullivan (2009), where further details can be found therein.

The experiments that inspired our apparatus design were paper burning experiments (Zhang *et al.* 1992; Maunuksela *et al.* 1997, 1999). These experiments consisted of burning optical lens tissue paper soaked with potassium nitrate (KNO_3, or more commonly known as saltpeter) for flameless, uniform, slow smoldering. They positioned the paper vertically, and ignited the paper from below by a straight heating wire to ignite the full length of the bottom edge. They measured the fire spread using four cameras (512×720 pixel movies) to obtain multi-level grayscale images that were later combined using software into a composite image (512×3000) for each frame. The experiments were designed to provide data to fit the Kardar–Parisi–Zhang nonlinear stochastic PDE model (Kardar, Parisi, and Zhang 1986) to study the variance of a growing linear fire front known as kinetic roughening.

An objective of previous research is to use an experimental burning apparatus to simulate forest fires at the local level. We conclude this literature review by pointing out there is a dearth of literature on simulating regional forest fire satellite imagery using experimental data. Our fire spread apparatus is designed to simulate fire spread over a region, where the fire spread is recorded using a satellite perspective. Our fire image measurements from level and sloped burns give insight into fire spread rates and uncertainties over a region. We demonstrate that the fire spread measurements can be processed into fire spread data and the processed fire spread data is analyzed to estimate local fire spread rates over the course of one fire.

In Section 2, we outline the design and experimental procedure of a fire smoldering apparatus, with an in-depth investigation into our choice of fuel bed. In Section 3, we use an anisotropic diffusion filter to denoise the fire spread measurements. In Section 4, we estimate the fire spread rates using data sharpening and kernel smoothing. To conclude, Section 5 is a summary of our results and a discussion about the contribution of our methodology to forest fire laboratory experiments.

2. Fire smoldering apparatus and experimentation

A micro-fire spread apparatus that measures paper smoldering experiments provides us with measurements, under controlled environmental conditions, that allow for a mouse model investigation of wildfire spread. The measurements can be processed, using statistical techniques, into different forms of data for the statistical analysis of fire spread mean behaviour and variability. Fire spread rates can be estimated from each smoldering experiment, and those estimates can be used to calibrate a fire growth model, and quantify spread rate estimation and model performance. Each experiment has controlled environmental conditions (e.g. elevation, moisture level, surface wind speed, and ignition location) and uncontrolled conditions (e.g. the local inconsistency of the wax paper manufacturing and local smoldering susceptibility from the non-uniform coating of potassium nitrate). The effects of the uncontrolled conditions, such as local inhomogeneity of the wax paper fibers and potassium nitrate coating, simulate the natural local randomness in the fuels of a forest fire.

From our experience, an apparatus for studying fire spread must meet the following conditions: First, the apparatus must incorporate both random and deterministic controls that are known within each experiment, and reproducible between experiments. This is accomplished through both the apparatus design, incorporating different configurations of the experiment, and the procedure of every experiment. Second, the apparatus measures the fire spread of a fully smoldering experiment. The measurements are recorded by a camera positioned over the experiment, and a potassium nitrate coating ensures smoldering to prevent large flames from blocking the view of the fire front. Smoke occlusion of the fire front can be mitigated by image processing methods that we have developed. Third, the apparatus must simulate fire spread scenarios with consistent environmental conditions. A fume-hood provides a fire-safe space with a consistent environment, and a tested experimental procedure allows for consistent control over fuel moisture, fuel type, and application of a potassium nitrate coating. Lastly, the apparatus must provide novel raw data that can be analyzed to provide insight into fire spread rate estimation, particularly the current challenges of modelling fire spread variability and firebrand spotting. The statistical methods developed herein process measurements into a new data set that did not previously exist for studying fire spread.

2.1. Apparatus description

Figure 1 shows the smoldering apparatus mounted in a laboratory fume hood (H.H. Hawkins Ltd. 111-72PR). The apparatus base is a nonflammable solid anodized aluminum optical breadboard (Newport) with dimensions $12 \times 18 \times 0.5$ inch, with 1/4-20 mounting holes on a 1 inch grid. An optical breadboard allows for consistent and controlled configurations of the experiment, and seamlessly integrates with mounting and camera equipment. Optical breadboard handles (Newport) allow for a fully set-up experiment to be easily moved inside the fume hood for experimentation. A $15.25 \times 10.25 \times 0.75$ inch metal tray is used to contain the smoldering paper experiment. To reduce glare off the bottom of the tray as observed in early experimental trials, the tray is coated in black heat-resistant paint to improve data extraction.

The metal tray has holes machined into the base to allow for mounting on supports, airflow to

Figure 1: A fire smoldering experiment in action, using a 32° slope configuration. The camera position in this figure is not the current standard. Here the camera is pointed orthogonal to the tray, but all experiments considered in this dissertation have the camera pointed orthogonal to the ground.

the smoldering experiments from below, and initiate smoldering by flame from underneath the try bed. The tray is supported by nonflammable, passivated stainless steel optical mounting posts (Newport). The camera (Olympus Stylus 600) is mounted on similar posts which hold it 19 inches above the center of the smoldering experiment, and pointed down and orthogonal to the ground. The camera captures 320 $\times$ 240 pixel images at 15 frames per second, and the spatial resolution of the camera for this experiment is approximately 1.2 mm.

The apparatus can be configured for level and sloped experiments by using different sets of mounting holes on the metal tray with different combinations of mounting post lengths. The apparatus currently has three slope configurations: 0°, 11°, and 32°. The 11° angle configuration was chosen to be just slightly different than a horizontal regime, and the 32° angle was chosen to be significantly different from the other two configurations. Figure 1 shows a smoldering experiment being run with the apparatus in a 32° slope configuration.

2.2. Wax paper and potassium nitrate coating

A major factor behind fire spread that is often discussed in the forest fire research literature is the fuel bed and mitigating environmental effects on the fuel bed Sullivan (2009). An ideal fuel bed contains local inhomogeneity of fuel with no discernible macroscopic patterns, is susceptible to local inhomogenous burning, does not require large energy to ignite when coated in potassium nitrate, contrasts white fuel with red burning and black burnt-out areas in measurements, is safe to work with inside a fume hood, and is cost-effective. Ultimately, the fuel bed used was wax paper since it satisfied all of these criteria and had the added benefits of having minimal flame-ups with a potassium nitrate coating, did not absorb an excessive amount of potassium nitrate or water, held its overall structural integrity during preparation and experimentation, and introduced appropriate levels of measurement noise. The wax paper consists of paper fibers coated in paraffin wax. To get a better idea of the local inhomogeneous structure and confirm claims about the microscopic structure, microscopic images of burnt and unburnt coated and uncoated wax paper were taken using scanning electron microscopy.

Wax paper was imaged using a Hitachi S-3400N SEM at the University of Western Ontario's Integrated Microscopy lab. The wax paper samples are prepared for the SEM by first sputter coating them in an ultra-thin gold/palladium layer. The gold/palladium coating makes the surface conductive to prevent the build-up of charge and to increase the production rate of secondary electrons that increase the amount of information when forming images. The gold/palladium coating is commonly used for imaging non-conductive materials with an SEM, as the metal layer allows electric charge to dissipate, protects the material's surface, and increases signal-to-noise since there are no electric fields (caused by charge build-up) present.

The local inhomogeneity of wax paper and the non-uniform coating of potassium nitrate are the main source of variation in the fire smoldering experiments, and simulate the local, fine-scale heterogeneity crucial to simulating realistic fire spread. The next set of figures shows the inhomogeneity of wax paper, with and without the potassium nitrate coating. Figure 2 shows the local non-uniform direction of the fibers at the microscopic scale and the torn edges of the wax paper, where we can further see the fibers' non-uniform sizes. The fibres sizes range in sizes around 30 μm and the paper fibers have no local microscopic weaving pattern and do not have a uniform wax coating. The digital camera's pixel resolution in our experimental apparatus is 1.2 mm and the local inhomogeneity is lost by the resolution during measurement similar to forest fuel data's spatial resolution (Braun, Jones, Lee, Woolford, and Wotton 2010). Additionally for Figure 2, note that the fibers do not appear to have chemically reacted with the wax.

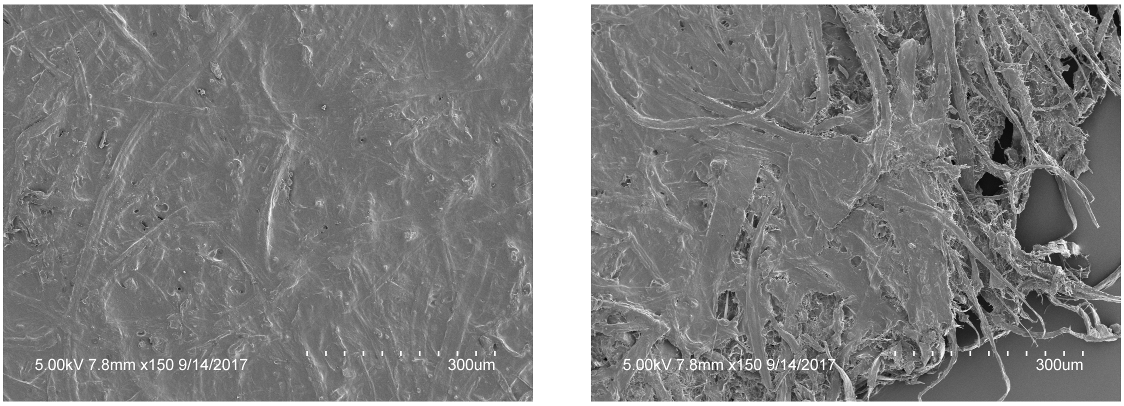

Figure 2: SEM images of the uncoated wax paper. Note that for all SEM images, the distance on the scale (300 μm) is for the entire length of the scale.

Figure 3 shows that the potassium nitrate coats the fibers and does not appear to react with the wax or fibers. This imagery supports the claim that the potassium nitrate does not react with paper during the coating process. Figure 4a shows the thickness of the wax paper through a torn edge. Figure 4b shows the thickness of the potassium nitrate coating, and how the potassium nitrate coats the surface of the wax paper and does not penetrate the fibers or wax. This is further evidence that the potassium nitrate does not react with the wax paper.

Figure 5 shows a piece of wax paper that was burned before applying the gold/palladium layer.

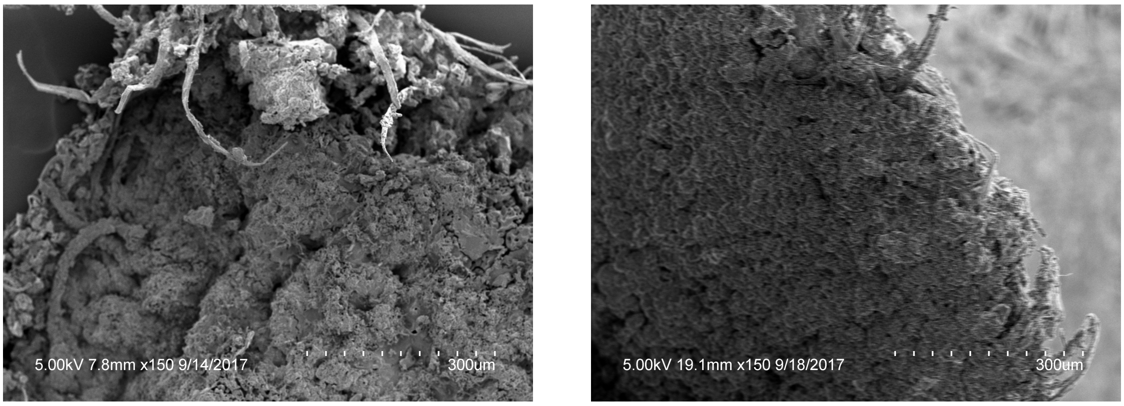

(a) Lying flat

(b) Slight angle

Figure 3: SEM images of the edge of wax paper coated in potassium nitrate.

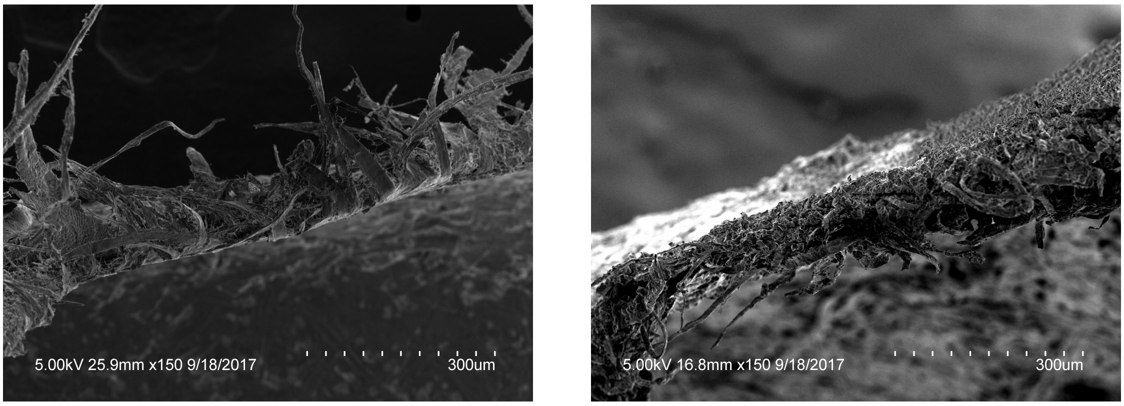

(a) Uncoated

(b) Coated

Figure 4: SEM images of thickness of wax paper, with and without the potassium nitrate coating.

Figure 5 when compared to Figure 2 shows that the structure of the fibers has remained intact through combustion, but the integrity of the paper is compromised and it crumbles. The wax around the burned paper has melted or evaporated, as evidenced by the newly formed holes on the surface. The view of the edge in Figure 5 shows a similar story where the wax has been melted or evaporated inside the wax paper. Figure 6 shows a flake of burned wax paper being held by paper fibers to the main body. This shows that even though the area is burnt, the remaining wax binds the burnt paper fibers together. The clumping of residual wax after burning is evidence of a firebrand phenomena that was found in experimentation. The black colour of the burnt paper suggests leftover carbon from combustion, which we believe makes up the residual fibers after burning. Figure 7 shows the clumping of the wax and fibers that formed around the burning edge and the clumps appear the clumps are actually more “hollow” than they appear macroscopically. The melting of the wax and potassium nitrate has caused the burning regions to clump. The oxygen from the melted potassium nitrate and airflow through holes is feeding the combustion reaction inside the clump, but the lower abundance of oxygen slowed the combustion reaction and created smoke from incomplete combustion.

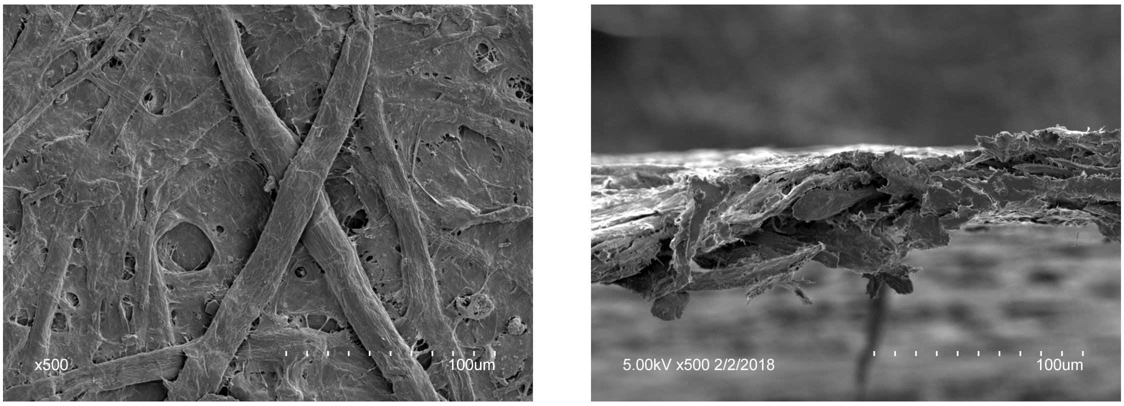

Figure 5: SEM images of burned uncoated wax paper.

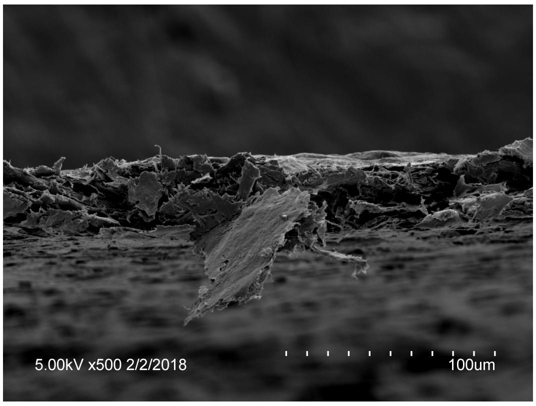

Figure 6: SEM images of burned wax paper with flaking.

These slow-burning clumps break off and carried aloft from local air turbulence, becoming firebrands that land on unburnt areas away from the fire front. This series of mechanisms creates an environment more likely to experience firebrand spotting.

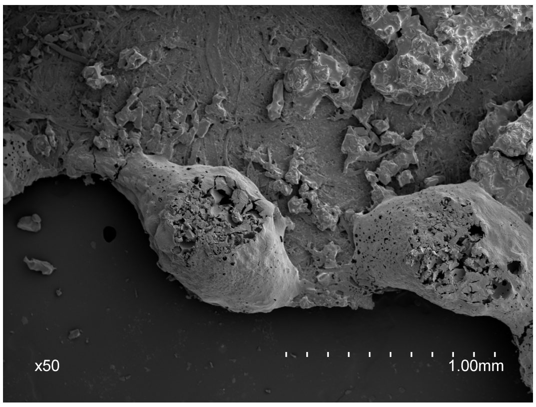

Figure 7: SEM images of burned coated wax paper with clumping.

2.3. Experimental procedure

The experimental set-up begins with cutting a sheet of wax paper to the same size as the tray and soaking the sheet in a 10 mL/g H_2O/KNO_3 solution inside a deep metal tray for 30-60 minutes. Inside the fume hood, the soaked paper is dried using a warming element set to 50-70°F for 60 to 120 minutes. The varying times and temperatures did not have an effect on the burning patterns. However, drying temperatures and times lower than these ranges had premature extinction or would not ignite. The dried potassium nitrate coated wax sheet is attached edge-to-edge onto the tray using paper tape, and the apparatus is assembled and placed inside the fume hood. With the camera recording and pointed down and orthogonal to the ground, the sheet is ignited using a directable ignitor from below through the holes in the bed of the tray and the smoldering is closely monitored. The experiment ceases when the experimenter extinguishes the flame with water from a spray bottle.

The movies from each experiment are cropped to remove any boundary areas that are not part of the smoldering area, e.g. edges of the tray or paper tape that attaches the coated wax paper to the tray. The trimming of the border prevents any undesirable false burning recognition and boundary effects during image processing. The movies are cropped in time to only include start to finish of each smoldering experiment. Additionally, frames are removed when the flame from the ignitor appears in the movie, as those frames cause errors in the "baseline" of a fire movie for processing. Finally, movies are segmented such that we only keep the first frame of each second. This introduces uncertainty of fire spread between images similar to the time between satellite images of a forest fire. Figure 8 shows one fire smoldering experiment after ignition at three points in time. Notice that the smoke occlusion of the experiment increases as the amount of smoldering increases. The uneven coating of potassium nitrate can be seen in white discolorations on the paper. These white spots show inhomogeneous oxidation control of burning areas over local smoldering regions of the fire front. With a plethora of raw measurement data in hand, we process the measurements into useful data formats.

3. Processing measurements into fire spread data

Figure 9 shows a raw unprocessed image and a visualization of the red channel values that demonstrates the variability over space. The RGB colour channels are similar throughout, except around the burning regions where the red channel differs substantially from the green and blue channels around the burning region in a fire image. When the white paper changes from fuel to burning, the camera reads it as a decrease in blue and green and an increase in red. When the burning paper extinguishes, the red channel decreases.

The fire images contain regions that are distinguished by boundaries or "edges" in an image, and we are interested smoothing in-between the boundaries. Anisotropic diffusion filtering is a partial differential equation (PDE) method for edge-preserve smoothing between boundaries that is a more general version of (isotropic) Gaussian filtering (Koenderink 1984; Hummel 1987). A mathematical interpretation of anisotropic diffusion is that it takes a convolution of the image and an isotropic kernel function, using an edge-stopping function to preserve boundaries between regions without supervision. The PDE for anisotropic diffusion is a more

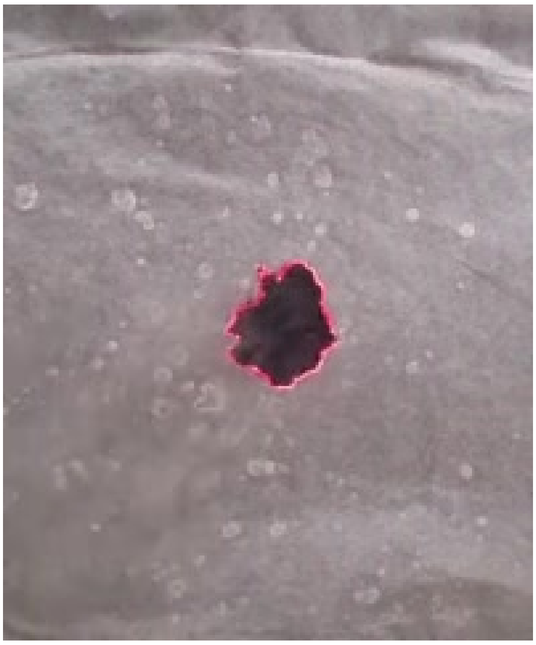

(a) Fire image at ten seconds

(b) Fire image at twenty seconds

Figure 8: Fire spread images from the 11° slope experiment 2.

(a) Original smoldering image

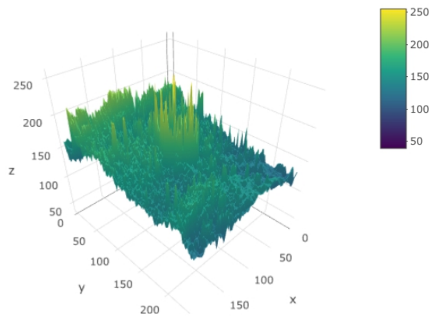

(b) Red channel

Figure 9: A fire spread image from ten seconds into the 11° experiment 2. The red RGB channel values are shown separately next to the original image. The z-axis is the red RGB channel value, and (x, y)-directions are the pixel locations of the image.

general version of the heatflow diffusion equation given by

$$\frac{\partial I(x,y,t)}{\partial t} = \nabla \cdot [f(\|\nabla I\|)\nabla I] \, ,$$

where $\nabla\cdot$ is the divergence operator, the edge-stopping function is $f(\|\nabla I\|) \to 0$ as $\|\nabla I\| \to \infty$, and initial condition $I(x,y,0)$ of the PDE is the original image. This PDE has no analytical solution for most initial and boundary conditions, but the behaviour of the system is approximated by a numerical solution. The anisotropic diffusion software (Pilny and Janacek 2006) uses an algorithm based on a framework for image regularization (Tschumperle and Deriche 2005).

An example of calculating an iterative solution for the anisotropic diffusion filter on a fire image is shown in Figure 10. The images appear to be blurred, and we visually identify three distinct fairly uniform colour regions of fuel (grey), burning (red), and burnt-out (black). The boundaries between regions are preserved, but are interrupted by smoke occlusion and oversmoothed by anisotropic estimators. The smoke occlusion increases as time increases since there is a larger burning area to produce more smoke. Figure 11 shows the result of anisotropic diffusion on each of the RGB channel values in the right column next to the original fire images in the left column, and we see how the noise of each region has been smoothed.

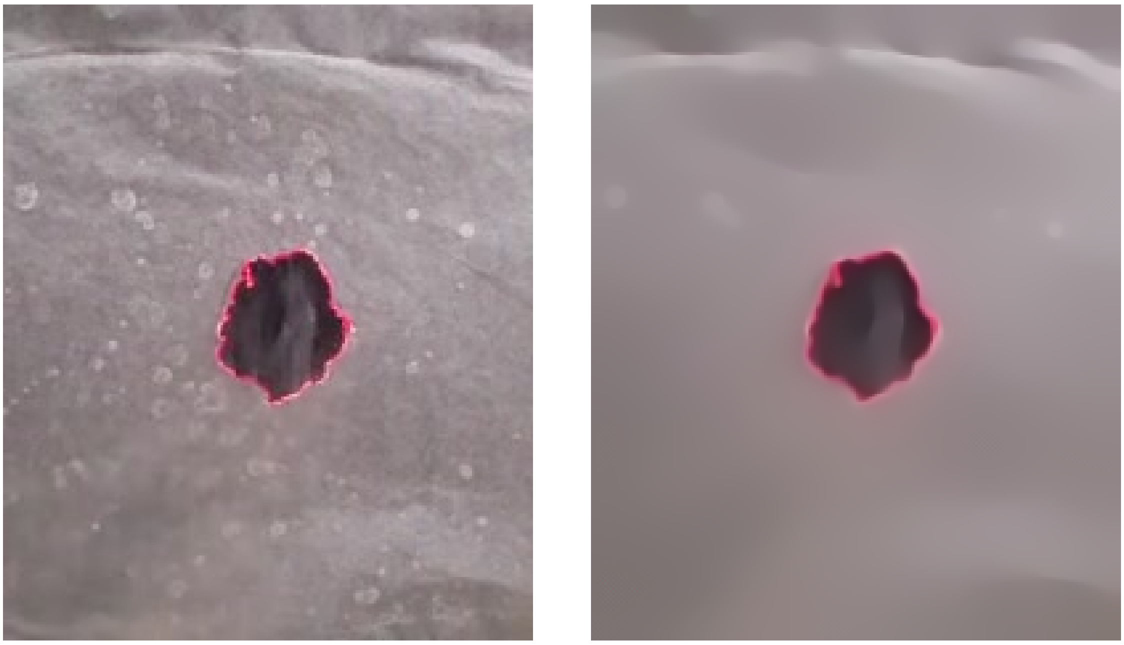

(a) Original image

(b) Anisotropic diffusions

Figure 10: The image result of applying an anisotropic diffusion filter on a smoldering image. The anisotropic diffusion procedure is 50 tensor field calculation iterations with 10 smooths per iteration.

4. Estimating fire rate of spread from smoothed measurements

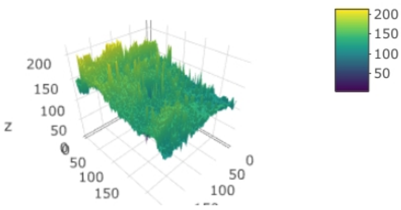

(a) Original image - Red

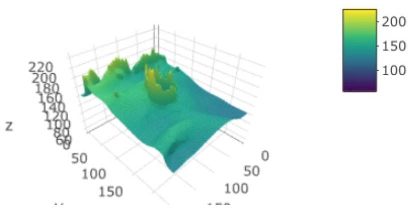

(b) Anisotropic diffusion - Red

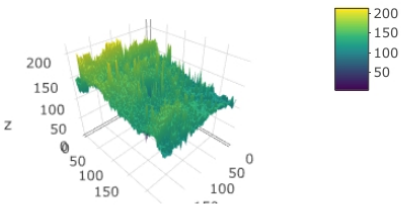

(c) Original image - Green

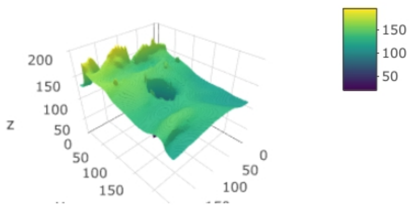

(d) Anisotropic diffusion - Green

Figure 11: The result for the RGB spectrum after applying image weighting and anisotropic diffusion on a smoldering image. The anisotropic diffusion procedure is 50 tensor field calculation iterations with 10 smooths per iteration. The z-axis is the RGB channel value, and (x, y)-directions are the pixel locations of the image.

Figure 12 shows the channel value of each RGB channel for one pixel over the course of the entire movie. The pixel RGB channels are not stationary, where there is a clear change in the mean value over time at ignition and extinction events, and there is a change in variance when the mean value changes. We also see an aberration, where the value jumps up to a 200 RGB value, after the ignition and extinction time change-points. The events of ignition and extinction are contained within the spike, however, those two event times are harder to resolve in the differenced image compared to considering each colour channel separately. To process and obtain the underlying data generating process of the fire spread images and process them, we smooth the surfaces in Figure 9 using anisotropic diffusion and local constant anisotropic smoothing such that we preserve the boundaries between the fuel, burning, and burnt-out regions of the fire image.

Data sharpening is used to improve the performance of statistical methods by perturbing the data to minimize a distance metric with the original data subject to constraints (Braun and Hall 2001). The data sharpening algorithm applied to the smoothed frame-by-frame data set is to minimize the distance metric of the sum of the squares of the Euclidean distance $\sum_{i=1}^{k}(r_j - r_j^*)^2$ between the red channel value of a pixel $r_j = r_j(x, y) \in [0, 255]$ and the sharpened data $r_j^* = r_j^*(x, y) \in [0, 255]$ subject to a set of constraints. The constraints are designed to estimate the ignition and extinction times that separate fuel, burning, and burnt-out states of a pixel. The pixel's state transitions from fuel to burning at the ignition time t_I, and from burning to burnt-out at the extinction time t_E. The red channel transitions at the

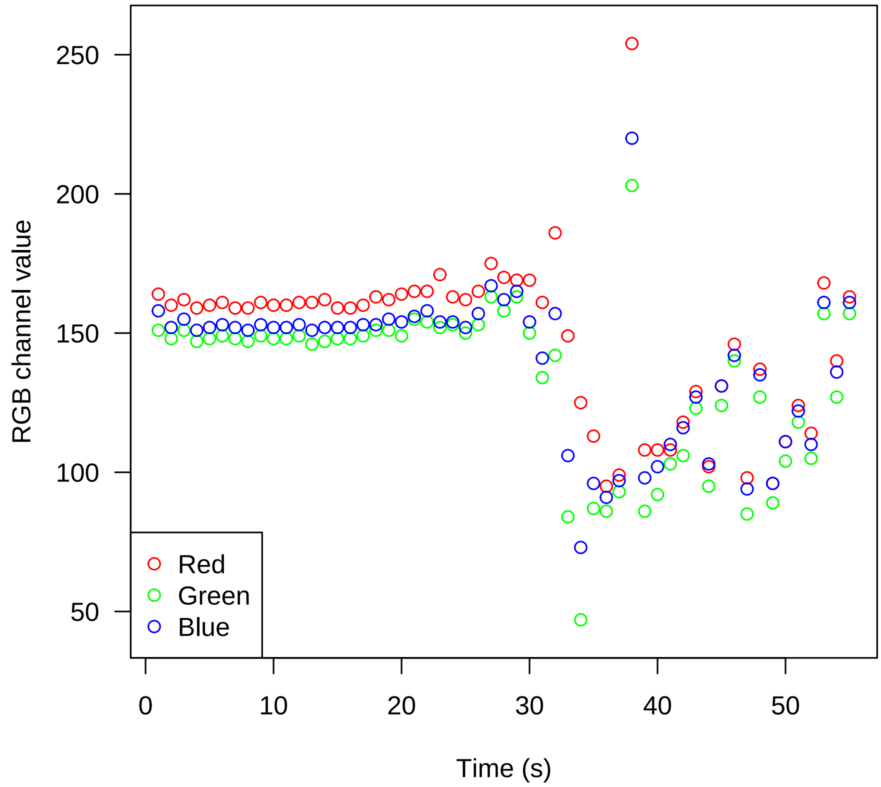

Figure 12: The red, green, and blue channel values of single pixel over the course of the 11° slope experiment 2.

time of extinction and green transitions at the time of ignition, and we write the transitions as linear constraints on the pixel at location (x, y) using

$$\textit{Red}\begin{cases}\text{Fuel \& burning:} & |r_j^* - c_1| < \epsilon, \quad 1 \le t_j \le t_E,\\ \text{Burnt-out:} & r_j^* \le \epsilon, \qquad t_j \ge t_E,\end{cases}$$

$$\textit{Green}\begin{cases}\text{Fuel:} & |g_j^* - c_1| < \epsilon, \quad 1 \le t_j \le t_I,\\ \text{Burning \& burnt-out:} & g_j^* \le \epsilon, \qquad t_j \ge t_I,\end{cases}$$

where g_j^* represents the green channel value. For this algorithm, we found that the effective parameter values for our data set are $c_1 = c_1(x, y) = r_1(x, y) + 70$–$r_1(x, y)$ is the first red value of a pixel at (x, y)–and $\epsilon = 10$.

To find the optimal ignition and extinction times using these parameter values, the quadratic objective function is minimized separately for each colour channel's constraint set. The sharpened data r_j^* that yields the objective function that is minimum for all constraint sets is considered the solution to this minimization problem. However, we are not directly interested in the optimal values of the sharpened data r_j^*, but rather the values of t_I and t_E that yield the optimal values of the large changes in r_j^*.

Figure 13 shows a perspective plot of the estimated extinction times from a fire movie. The area of fire ignition starts around a point near the base of the event time surface and spreads as a warped cone as time increases. The shape demonstrates good performance near the beginning (the base of the cone) and generally poorer performance as time progresses to the end of the video. The evidence of poor performance is the long vertical regions where ignition times are relatively large between neighbouring pixels. We know, by comparing with the raw images, that there is significant spread outwards at these long vertical regions. Inspection of the channel values over time at these neighbouring pixels revealed that the inaccuracy in estimation is caused by smoke occlusion–the amount of smoke increases as the amount of smoldering material increases– that interrupts the signal from the true image to the camera.

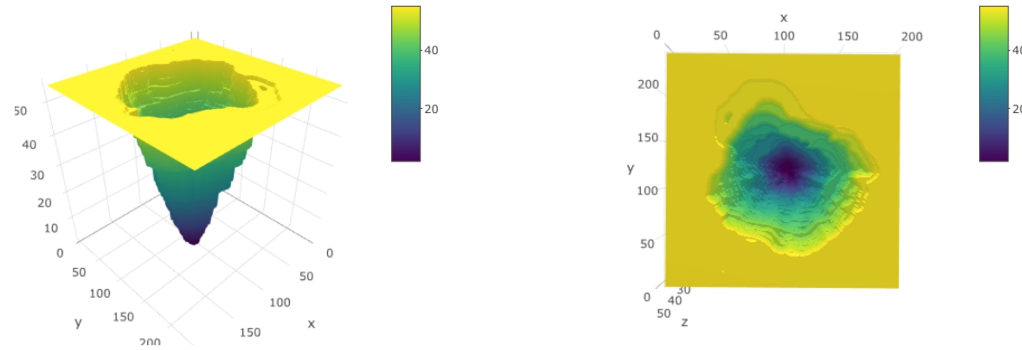

Figure 13: The ignition event times estimated using data sharpening for 11° slope fire experiment 2. The z-axis is time, and (x, y)-directions are the pixel locations of the movie.

We note that the ignition times estimated by data sharpening have systematic errors inside of the burning regions in some videos. This problem is mitigated through the intelligent choice of c_1. Using static (c_1 is constant for each pixel of a movie) or adaptive (c_1 changes for each pixel of a movie) parameter values both yielded results that contained regions of ignition and extinction time with some errors, where adaptive outperforms static parameter choice. We find that choosing the first pixel value in the time sequence plus a constant between 70 and 100, i.e. $c_1(x, y) = r_1(x, y) + 70$, yielded an improved estimate.

We found that errors occur during data measurement and these errors do not compound on errors from the data sharpening algorithm–the statistical estimation error is largely independent of the measurement error. The sources of noise arise from systematic problems that include smoke occlusion, flare-ups, ambient laboratory light, automatic internal adjustments of the camera such as re-focusing. Additionally, the discrete nature of the data means that the exact moment of ignition is unlikely to be captured in one of the frames of the recording. Even with this measurement noise present, we have demonstrated that our methods are capable at estimating ignition and extinction times.

Figures 13 shows the estimated ignition times of each pixel location of a fire video. The discrete format of the ignition event time estimates cannot be used to calculate the instantaneous spread rates at each pixel location. The functional form of the ignition time surface across space is not known, but the warped cone shape for ignition times is found across all movies. We know that the ignition of a pixel must have occurred during the time interval between being a fuel cell and burning. To estimate the data generating process of ignition times, we use the local constant kernel estimator given by

$$\widehat{g}(x) = \frac{\sum_{i=1}^{n} Y_i K\left(\frac{X_i - x}{h}\right)}{\sum_{i=1}^{n} K\left(\frac{X_i - x}{h}\right)}, \tag{1}$$

where the function K is a multivariate kernel function. This allows us to estimate the ignition and extinction time surface between the pixel locations. The derivative of this estimate yields the instantaneous fire spread rate at each pixel location. The upper plot of Figure 14 shows the local constant estimate of the data from Figure 13. The figure demonstrates how the "roughness" from the discrete data is smoothed, and intra-pixel values are smoothed and no longer constant.

Instantaneous spread rates are calculated by taking the derivative of the Equation (1), given by

$$\frac{\partial}{\partial x}\widehat{g}(x) = \frac{1}{h\sum_{j=1}^{n} K\left(\frac{X_j - x}{h}\right)}\left[-\sum_{i=1}^{n} Y_i K'\left(\frac{X_i - x}{h}\right) + \frac{\sum_{i=1}^{n} Y_i K\left(\frac{X_i - x}{h}\right)\sum_{j=1}^{n} K'\left(\frac{X_j - x}{h}\right)}{\sum_{j=1}^{n} K\left(\frac{X_j - x}{h}\right)}\right].$$

Figure 14 shows a filled contour plot of the ignition times and the vector field of the estimator's gradient $\frac{\partial}{\partial x}\widehat{g}(x)$ in the level plot. The contour map represents the inverse of the magnitude of the spread rates $\left|\frac{\partial}{\partial x}\widehat{g}(x)\right|^{-1}$ and the vector field shows the direction. For the vector field, this implies that the shorter the arrow, the larger the spread rate. The areas that are never burned around the fire spread area are reporting very large spread rates. These areas are not the areas of interest.

5. Discussion

The paper smoldering experiments described in this research are similar to the experiments performed by (Zhang *et al.* 1992), except for a few key differences. First, wax paper is used in place of optical lens cleaning tissue. Wax's hydrophobic nature prevents large amounts of moisture from being retained in the material during soaking, which decreases preparation time and reduces the amount of potassium nitrate bound within the paper fibers. Our preliminary experiments showed that excessive potassium nitrate deposits cause premature extinction of smoldering. Second, previous videos (Zhang *et al.* 1992) were recorded using a higher resolution camera, with an effective pixel grid of 512×3000 that is much larger than our pixel grid of 320×240. Lastly, the purpose of their videos was to investigate an interface growth model of a linear fire front, whereas we are interested in determining the fire rate of spread distributions over a fire that burns radially outward from a point of ignition. Our analysis work is similar in the processing and analysis of the infrared data to study fire streak structure of Miller, Tang, Finney, McAllister, Forthofer, and Gollner (2017), where interests centers on identifying specific regions of the data. Our methods could be applied to smooth those streak regions and find the change-point boundaries of flame and non-flame for fire structure.

An issue throughout experimentation and data analysis is smoke occlusion. To remove occlusion caused by smoke so that we can better identify fuel, burning, and burnt-out regions, images could be weighted by the previous time stamp image. An area occluded by smoke in

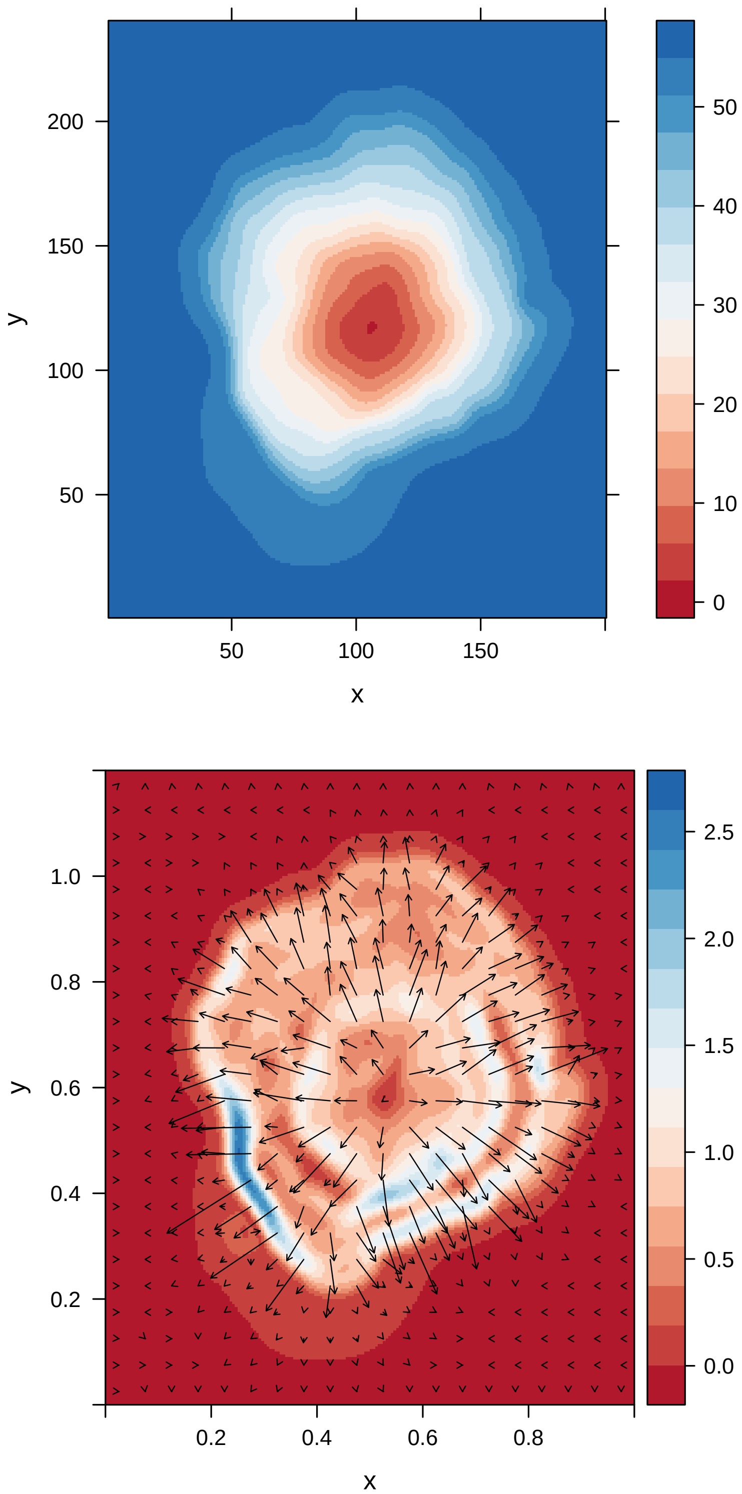

Figure 14: The upper plot is the local constant smoothed ignition times in a level plot. The smoothing was conducted using the `np` package's (Hayfield and Racine 2008; R Core Team 2018) local constant estimator with least-squares cross-validation (Hurvich *et al.* 1998) for bandwidth selection on the ignition time data in Figure 13. The (x, y)-directions are the pixel locations and the colour gradient is time. The colour gradient in the lower plot is the magnitude of the inverse of fire spread rates. The inverse of fire spread rates are displayed as a vector field calculated from the gradient for the smoothed ignition time surface of $11°$ slope experiment 2. Note that the size of the vector is inversely proportional to the spread rate.

the current image may not be occluded in the previous image. Therefore, burnt-out aberrant points in a pixel's channel values would have a value close to black after being re-weighted. This re-weighting was performed on some movies with mixed results, however, the optimal re-weighting of images was not thoroughly pursued and remains an avenue for future work. The data sharpening and kernel smoothing methods used to estimate ignition and extinction event times during the late stages of smoldering experiments. These issues seem to be caused by smoke, which occludes the ignition and extinction events and thus we have poor estimations for spread rates during the late stages of an experiment when the amount of smoke generated is substantial.

The data sharpening algorithm can be viewed as change-point location estimation. We omit a lengthy and in-depth literature review on change-point location estimation, as we are not evaluating our change-point location estimation procedure against other methods. We are interested in the change-point estimation task at hand, and while many methods exist for estimating change-point location, none are specifically designed for this task. Additionally, there is no literature that uses data sharpening as a method to estimate change-point locations and therefore the application of these methods are novel. Therefore, we submit that data sharpening is used in this paper as a change-point location estimator, and studying data sharpening for that purpose is another avenue of future work.

We have shown that fire spread rates can be estimated from each smoldering experiment's processed measurements. We found that data sharpening can estimate ignition and extinction time events at the pixel level in fire spread images, and kernel smoothing estimates intra-pixel ignition and extinction time that allow for the estimation of fire spread rates. These fire spread rate estimates can be used to calibrate a fire growth model, and quantify model and spread estimation performance. Each experiment is conducted with controlled conditions, such as elevation, surface wind speed, and ignition location, and uncontrolled conditions, such as local inconsistency of the wax paper manufacturing and local smoldering susceptibility from the non-uniform coating of the potassium nitrate. The effects of the controlled conditions are observed in the directional rates of burning; simply, fire spreads faster when it moves uphill and slower downhill. The effects of the uncontrolled conditions attempt to capture the uncertainty of forest fire spread.

Acknowledgements We thank Karen Nygard and the Integrated Microscopy lab at Western University for the instruction and usage of their scanning electron microscope. We also thank Andrew J. Jirasek at the University of British Columbia Okanagan for allowing us to use his laboratory space for fire smoldering experiments and his insightful comments on experimental methodology. Finally, we would like to gratefully acknowledge Doug G. Woolford for his comments on this manuscript. This research was supported by funding from the Natural Sciences and Engineering Research Council, the Canadian Statistical Sciences Institute, and the Institute for Catastrophic Loss Reduction.

References

Beer T (1993). "The speed of a fire front and its dependence on wind-speed." *International Journal of Wildland Fire*, **3**(4), 193–202.

Beer T (1995). "Fire Propagation in Vertical Stick Arrays-the Effects of Wind." *International Journal of Wildland Fire*, **5**(1), 43–49.

Braun WJ, Hall P (2001). "Data Sharpening for nonparametric inference subject to constraints." *Journal of Computational and Graphical Statistics*, **10**(4), 786–806.

Braun WJ, Jones BL, Lee JS, Woolford DG, Wotton BM (2010). "Forest fire risk assessment: an illustrative example from Ontario, Canada." *Journal of Probability and Statistics*, **2010**.

Buscarino A, Famoso C, Fortuna L, Frasca M, Xibilia MG (2015). "Complexity in forest fires: From simple experiments to nonlinear networked models." *Communications in Nonlinear Science and Numerical Simulation*, **22**(1-3), 660–675.

Catchpole W, Catchpole E, Butler B, Rothermel R, Morris G, Latham D (1998). "Rate of spread of free-burning fires in woody fuels in a wind tunnel." *Combustion Science and Technology*, **131**(1-6), 1–37.

Couffinhal T, Silver M, Zheng LP, Kearney M, Witzenbichler B, Isner JM (1998). "Mouse model of angiogenesis." *The American journal of pathology*, **152**(6), 1667.

Cruz M, Alexander M (2013). "Uncertainty associated with model predictions of surface and crown fire rates of spread." *Environmental Modelling & Software*, **47**, 16–28.

Finney MA, Cohen JD, Forthofer JM, McAllister SS, Gollner MJ, Gorham DJ, Saito K, Akafuah NK, Adam BA, English JD (2015). "Role of buoyant flame dynamics in wildfire spread." *Proceedings of the National Academy of Sciences*, **112**(32), 9833–9838.

Finney MA, Forthofer J, Grenfell IC, Adam BA, Akafuah NK, Saito K (2013). "A study of flame spread in engineered cardboard fuelbeds: Part I: Correlations and observations." In *In: Seventh International Symposium on Scale Modeling (ISSM–7); Hirosaki, Japan; 6-9 August, 2013. International Scale Modeling Committee. 10 p.*

Finney MA, Forthofer JD, Grumstrup TP (2017). "Wind and Slope effects on Flame Scaling in Laboratory Fires." In *Eighth International Symposium on Scale Modeling (ISSM–8); Portland, Oregon, USA; 12-14 September, 2017.*

Fons WL (1946). "Analysis of fire spread in light forest fuels." *Journal of Agricultural Research*, **72**(3), 93–121.

Hayfield T, Racine J (2008). "Nonparametric Econometrics: The **np** Package." *Journal of Statistical Software*, **27**(5). URL http://www.jstatsoft.org/v27/i05/.

Hummel RA (1987). "Representations based on zero-crossings in scale-space." In *Readings in Computer Vision*, pp. 753–758. Elsevier.

Hurvich C, Simonoff J, Tsai C (1998). "Smoothing parameter selection in nonparametric regression using an improved Akaike information criterion." *Journal of the Royal Statistical Society B*, **60**, 271–293.

Hwang C, Xie Y (1984). "Flame Propagation Along Matchstick Arrays On Inclined Base Boards." *Combustion Science and Technology*, **42**(1-2), 1–12.

Kardar M, Parisi G, Zhang YC (1986). "Dynamic scaling of growing interfaces." *Physical Review Letters*, **56**(9), 889.

Koenderink JJ (1984). "The structure of images." *Biological cybernetics*, **50**(5), 363–370.

Maunuksela J, Myllys M, Kähkönen OP, Timonen J, Provatas N, Alava M, Ala-Nissila T (1997). "Kinetic roughening in slow combustion of paper." *Physical review letters*, **79**(8), 1515.

Maunuksela J, Myllys M, Timonen J, Alava M, Ala-Nissila T (1999). "Kardar–Parisi–Zhang scaling in kinetic roughening of fire fronts." *Physica A: Statistical Mechanics and its Applications*, **266**(1-4), 372–376.

Miller CH, Tang W, Finney MA, McAllister SS, Forthofer JM, Gollner MJ (2017). "An investigation of coherent structures in laminar boundary layer flames." *Combustion and Flame*, **181**, 123–135.

Pilny V, Janacek J (2006). *Anisotropic Diffusion 2D v0.3.* Accessed on April 2nd 2017, URL https://imagej.nih.gov/ij/plugins/anisotropic-diffusion-2d.html.

Prahl J, Tien J (1973). "Preliminary investigations of forced convection on flame propagation along paper and matchstick arrays." *Combustion Science and Technology*, **7**(6), 271–282.

R Core Team (2018). *R: A Language and Environment for Statistical Computing.* R Foundation for Statistical Computing, Vienna, Austria. URL https://www.R-project.org/.

Rothermel RC, Anderson HE (1966). *Fire spread characteristics determined in the laboratory.* Intermountain Forest & Range Experiment Station, Forest Service, US Department of Agriculture.

Sullivan AL (2009). "Wildland surface fire spread modelling, 1990–2007. 2: Empirical and quasi-empirical models." *International Journal of Wildland Fire*, **18**(4), 369–386.

Tschumperle D, Deriche R (2005). "Vector-valued image regularization with PDEs: A common framework for different applications." *IEEE transactions on pattern analysis and machine intelligence*, **27**(4), 506–517.

Vogel M, Williams F (1970). "Flame propagation along matchstick arrays." *Combustion Science and Technology*, **1**(6), 429–436.

Weise D, Biging G (1994). "Effects of wind velocity and slope on fire behavior." *Fire Safety Science*, **4**, 1041–1051.

Wolff M, Carrier G, Fendell F (1991). "Wind-aided firespread across arrays of discrete fuel elements. II. Experiment." *Combustion Science and Technology*, **77**(4-6), 261–289.

Zhang J, Zhang YC, Alstøm P, Levinsen M (1992). "Modeling forest fire by a paper-burning experiment, a realization of the interface growth mechanism." *Physica A*, **189**, 383–389.

Affiliation:

John R.J. Thompson
Department of Mathematics, Wilfrid Laurier University
Waterloo, ON N2L 3C5
E-mail: johnthompson@wlu.ca

W. John Braun
Department of Computer Science, Mathematics, Physics and Statistics, UBCO
Kelowna, BC V1V 1V7
E-mail: john.braun@ubc.ca
URL: https://stat.ok.ubc.ca/faculty/braun.html

Journal of Environmental Statistics http://www.jenvstat.org
Volume 9, Issue 6 Submitted: 2018-11-1
April 2020 Accepted: 2020-05-14